



ISSN: 0975-833X

**RESEARCH ARTICLE**

**STRUCTURAL AND SPECTROSCOPIC CHARACTERIZATION OF 4-METHYLBELLIFERONE: A COMBINED EXPERIMENTAL AND COMPUTATIONAL STUDY**

\*<sup>1</sup>Raj, R. K., <sup>2</sup>Gunasekaran, S., <sup>3</sup>Gnanasambandan, T. and <sup>4</sup>Seshadri, S.

<sup>1</sup>Department of Physics, SCSVMV University, Enathur, Kanchipuram-631561

<sup>2</sup>Research and Development, St.Peter's University, Avadi, Chennai -600 054

<sup>3</sup>Department of Physics, Pallavan College of Engineering, Kanchipuram -631 502

<sup>4</sup>Department of Physics, L.N.Govt. Arts College, Ponneri-631562

<sup>1</sup>Departmet of Physics, Pachaiyappa's College for Men, Kanchipuram-631 503

**ARTICLE INFO**

**Article History:**

Received 24<sup>th</sup> February, 2015

Received in revised form

29<sup>th</sup> March, 2015

Accepted 07<sup>th</sup> April, 2015

Published online 31<sup>st</sup> May, 2015

**Key words:**

FTIR FT-Raman,  
DFT,  
MEP,  
NBO,  
NLO.

**ABSTRACT**

The FTIR and FT-Raman spectra of 4-methylumbelliferone (4MUB) have been recorded in the region 4000–400 and 3500–100 cm<sup>-1</sup>, respectively. The optimized geometry, frequency and intensity of the vibrational bands of 4MUB were obtained by the density functional theory (DFT) using 6-31G(2d,3p) and 6-311++G(2d,3p) basis sets. The harmonic vibrational frequencies were scaled and compared with experimental values. The observed and the calculated frequencies are found to be in good agreement. The UV-visible spectrum was also recorded and compared with the theoretical values. The calculated HOMO and LUMO energies show that charge transfer occurs within the molecule. The first order hyperpolarizability ( $\beta_0$ ), related properties ( $\beta$ ,  $\alpha_0$  and  $\Delta\alpha$ ) and the Mulliken charges of the molecule were also computed using DFT calculations. Stability of the molecule arising from hyperconjugative interactions, charge delocalization have been analyzed using natural bond orbital (NBO) analysis. The results show that charge in electron density (ED) in the  $\sigma^*$  and  $\pi^*$  antibonding orbitals and second order delocalization energies (E2) confirms the occurrence of intramolecular charge transfer (ICT) within the molecule. Information about the charge density distribution of the molecule and its chemical reactivity has been obtained by mapping molecular electrostatic potential surface.

Copyright © 2015 Raj et al. This is an open access article distributed under the Creative Commons Attribution License, which permits unrestricted use, distribution, and reproduction in any medium, provided the original work is properly cited.

**Citation:** Raj, R.K. Gunasekaran, S. Gnanasambandan, T. Seshadri, S, 2015. "Structural and spectroscopic characterization of 4-methylumbelliferone: a combined experimental and computational study", *International Journal of Current Research*, 7, (5), 16083-16092.

**INTRODUCTION**

Coumarin is a fragrant organic chemical compound in the benzopyrone chemical class, which is a colorless crystalline substance in its standard state. It is a natural substance found in many plants. The name comes from a French term for the tonka bean, *coumarou*, one of the sources from which coumarin was first isolated as a natural product in 1820. It has a sweet odor, readily recognised as the scent of new-mown hay, and has been used in perfumes since 1882. Coumarin and its derivatives were studied by several authors. Experimental Spectroscopic (FT-IR, FT-Raman, NMR) and DFT Studies of 7-methoxy-4-bromomethylcoumarin were studied by Prabavathi et al., ? FTIR, FT-Raman, FT-NMR and quantum chemical investigations of 3-acetylcoumarin were investigated by

Arjunan et al, (2013) Molecular structure, vibrational spectroscopic studies and natural bond orbital analysis of 7-amino-4-trifluoromethyl coumarin were reported by Subramanian et al, (2010) Scaled Quantum Chemical Calculations and FT-IR, FT- Raman Spectral Analysis of 4-Hydroxy-3-Nitrocoumarin were carried out by Sivasubramanian (2012) FT-IR, FT-Raman and UV-Vis spectra and DFT calculations of 3-cyano-4-methylcoumarin were studied earlier by N. Udaya Sri (2012). In the present work, harmonic-vibrational frequencies are calculated for 4-methylumbelliferone (4MUB) using B3LYP with 6-31G (2d, 3p) and 6-311++G(2d,3p) method. The calculated spectra of the compound are compared to that of experimentally observed FT-IR and FT-Raman spectra. The redistribution of electron density (ED) in various bonding and antibonding orbitals and E(2) energies have been calculated by natural bond orbital (NBO) analysis by DFT method to give clear evidence of stabilization originating from the hyper conjugation of various intramolecular interactions. The HOMO and LUMO analysis have been used to elucidate information regarding ionization

\*Corresponding author: Raj, R. K,

Department of Physics, SCSVMV University, Enathur, Kanchipuram-631561

Department of Physics, Pachaiyappa's College for Men, Kanchipuram-631 503

potential (IP), electron affinity (EA), electronegativity ( $\chi$ ), electrophilicity index ( $\omega$ ), hardness ( $\eta$ ) and chemical potential ( $\mu$ ) are all correlated. These are all confirming the charge transfer within the molecule and also molecular electrostatic potential (MESP) contour map shows the various electrophilic region of the title molecule. However, molecular hyperpolarizability is also calculated by DFT method.

parameters and vibrational wavenumbers of the normal modes of the title molecule. All the theoretical calculations were performed using the Gaussian 03W program (Gaussian, 2004) with the default convergence criteria, without any constraint on the geometry (Schlegel, 1982). The equilibrium geometry corresponding to the true minimum on the potential energy surface (PES) was effectively obtained by solving

**Table 1.** Optimized geometrical parameters of 4MUB

Bond length(Å)	B3LYP		Bond angle(°)		B3LYP	
	6-31G(2d,3p)	6-311++G(2d,3p)	6-31G(2d,3p)	6-311++G(2d,3p)	6-31G(2d,3p)	6-311++G(2d,3p)
C1-O2	1.203	1.203	O2-C1-C3	126.39	126.30	
C1-C3	1.451	1.449	O2-C1-O12	117.49	117.50	
C1-O12	1.395	1.395	C3-C1-O12	116.11	116.18	
C3-C4	1.355	1.353	C1-C3-C4	123.20	123.12	
C3-H14	1.083	1.079	C1-C3-H14	114.83	115.05	
C4-C5	1.449	1.447	C4-C3-H14	121.95	121.81	
C4-C13	1.503	1.501	C3-C4-C5	118.61	118.69	
C5-C6	1.405	1.403	C3-C4-C13	121.14	121.00	
C5-C11	1.410	1.406	C5-C4-C13	120.24	120.29	
C6-C7	1.384	1.381	C4-C5-C6	124.57	124.53	
C6-H15	1.083	1.080	C4-C5-C11	118.07	118.19	
C7-C8	1.403	1.400	C6-C5-C11	117.35	117.27	
C7-H16	1.085	1.082	C5-C6-C7	121.53	121.53	
C8-O9	1.358	1.362	C5-C6-H15	119.42	119.51	
C8-C10	1.391	1.387	C7-C6-H15	119.03	1118.95	
O9-H17	0.963	0.962	C6-C7-C8	119.67	119.63	
C10-C11	1.390	1.387	C6-C7-H16	120.38	120.31	
C10-H18	1.082	1.079	C8-C7-H16	119.94	120.04	
C11-O12	1.357	1.360	C7-C8-O9	122.44	122.29	
C13-H19	1.094	1.091	C7-C8-C10	120.34	120.46	
C13-H20	1.090	1.087	O9-C8-C10	117.20	117.24	
C13-H21	1.094	1.091	C8-O9-H17	109.47	109.94	
			C8-C10-C11	119.18	119.04	
			C8-C10-H18	120.67	120.78	
			C11-C10-H18	120.13	120.16	
			C5-C11-C10	121.89	122.04	
			C5-C11-O12	121.81	121.64	
			C10-C11-O12	116.29	116.30	
			C1-O12-C11	122.17	122.14	
			C4-C13-H19	111.05	111.04	
			C4-C13-H20	110.92	110.84	
			C4-C13-H21	111.03	111.02	
			H19-C13-H20	108.28	108.28	
			H19-C13-H21	107.12	107.21	
			H20-C13-H21	108.28	108.27	

## Experimental

The compound 4-methylumbelliferon (4MUB) was purchased from Sigma-Aldrich Chemical Company in the solid form with a stated purity of greater than 98% and it was used as such without further purification. The FTIR spectrum of the sample was carried out between 4000 cm<sup>-1</sup> and 400 cm<sup>-1</sup> on an IFS 66 V spectrometer using the KBr pellet technique. The room temperature, FT-Raman spectrum was recorded using a Thermo Electron Corporation model Nexus 670 spectrophotometer equipped with FT-Raman module accessory. The 1064 nm line of an Nd-YAG laser was used as excitation wavelength in the region of 3500–100 cm<sup>-1</sup>. The spectral resolution was set to 4 cm<sup>-1</sup> in a back scattering mode. A liquid nitrogen cooled Ge detector was used to collect 50 scans for a good Raman spectrum. The laser output was kept at 150mW for the solid sample.

## Computational details

In the present work, the density functional theory (DFT/B3LYP) at the 6-31G (2d,3p) and 6-311++G (2d,3p) basis sets level were adopted to calculate the optimized

self-consistent field equation. The vibrational spectra of the 4MUB were obtained by taking the second derivative of energy, computed analytically. The optimized structural parameters were used in the vibrational frequency calculations at DFT levels to characterize all stationary points as minima using the GAUSSVIEW animation program (Frisch *et al.*, 2000). Vibrational frequencies were computed at DFT level which had reliable one-to-one correspondence to experimental IR and Raman frequencies (Krishnakumar *et al.*, 2008). The vibrational assignments of the normal modes were made on the basis of the potential energy distribution (PED) calculated by using the VEDA 4 program (Jamroz, 2004). Subsequent potential energy distribution to each observed frequencies, predicts well the purity of the fundamental modes and shows the reliability and accuracy of the spectral analysis. In the present study, we have used the following scaling factor of 0.995 for B3LYP/6-31G (2d,3p) and 6-311++G(2d,3p) methods (<http://srdata.nist.gov/ccbdb/vsf.asp>). A comparison of the frequencies calculated with the experimental values revealed that the 6-31G (2d,3p) basis set result shows very good agreement with the experimental observations.

Table 2. Vibrational Assignments of 4MUB

Mode No.	Experimental		Calculated B3LYP		Vibrational Assignments + PED(%)
	FT-IR vcm <sup>-1</sup>	FT-R vcm <sup>-1</sup>	6-31G(2d,3p) Scaled vcm <sup>-1</sup>	6-311++G(2d,3p) Scaled vcm <sup>-1</sup>	
1	3649	-	3639	3637	vOH(98)
2	-	-	3215	3214	vCH(99)
3	-	-	3203	3203	vCH(99)
4	-	-	3200	3199	vCH(92)
5	-	-	3165	3165	vCH(94)
6	-	-	3128	3122	vCH <sub>3</sub> (83)
7	3091	3083	3086	3080	vCH <sub>3</sub> (99)
8	2924	2924	2935	2932	vCH <sub>3</sub> (99)
9	1825	-	1830	1823	vOC(83)
10	1694	1691	1683	1680	vCC(45)
11	-	-	1659	1655	vCC(47)
12	1610	1614	1609	1602	vCC(49)+ $\beta$ CCC(11)
13	1556	1554	1548	1543	vCC(10)+vOC(11)+ $\beta$ HCC(36)
14	1513	-	1495	1493	$\beta$ HCH(70)+ $\tau$ HCCC(20)
15	-	-	1488	1486	$\tau$ HCCC(10)+ $\beta$ HCH(82)
16	-	-	1481	1473	vCC(13)+ $\beta$ HCC(23)
17	1453	1457	1445	1443	vCC(11)+ $\beta$ HCH(42)
18	-	-	1406	1404	$\beta$ HCH(23)
19	1384	1367	1384	1368	vCC(40)
20	1342	-	1342	1339	vOC (37)
21	1312	1313	1297	1296	$\beta$ HCC(44)
22	1261	1269	1252	1254	vOC(10)+ $\beta$ HOC(29)+ $\beta$ HCC(11)
23	1248	-	1244	1233	vCC(10)+ $\beta$ HCC(42)
24	1209	1212	1198	1196	$\beta$ HCC(14)+ $\beta$ HOC(17)
25	1162	1161	1167	1166	$\beta$ HCC(51)
26	1145	-	1156	1147	$\beta$ HCC(15)+vOC(31)
27	1077	-	1078	1078	vCC(18)+ $\beta$ CCC(12)
28	1042	-	1052	1056	$\beta$ HCH(26)+ $\tau$ HCCC(51)+ $\gamma$ CCCC(14)
29	1012	1013	1019	1020	$\tau$ HCCC(28)
30	-	-	995	995	$\tau$ HCCC(22)
31	952	-	940	952	$\tau$ HCCC(83)
32	-	-	885	890	$\tau$ HCCO(12)+ $\tau$ HCCC(51)+ $\gamma$ OCOC(19)
33	-	-	880	881	$\tau$ HCCO(45)+ $\tau$ CCCC(11)+ $\gamma$ OCOC(10)
34	857	-	879	874	vOC(26)+ $\beta$ OCC(11)
35	820	-	810	812	vCC(12)+ $\beta$ OCO(16)
36	774	-	782	785	$\tau$ HCCC(54)+ $\gamma$ CCCC(11)
37	751	-	766	768	$\tau$ HCCC(34)+ $\gamma$ OCOC(13)+ $\gamma$ CCCC(13)
38	725	-	722	722	vCC(32)+vOC(10)+ $\beta$ CCC(12)
39	-	-	719	718	$\tau$ HCCO(25)+ $\gamma$ OCOC(46)
40	686	688	693	694	vCC(13)+ $\beta$ CCC(33)+ $\beta$ CO(11)
41	648	-	654	646	$\tau$ HCCC(26)+ $\gamma$ OCOC(53)
42	619	619	608	611	$\beta$ OCO(27)+ $\beta$ CCC(11)+ $\beta$ OCC(14)
43	569	569	560	560	vCCCC(39)+ $\gamma$ OCOC(19)
44	546	547	538	539	vOC(13)+ $\beta$ CCC(14)+ $\beta$ CO(11)+ $\beta$ OC(14)
45	-	-	497	498	$\beta$ CCC(36)
46	470	472	465	464	$\tau$ HCCC(12)+ $\tau$ CCCC(45)+ $\gamma$ OCOC(14)
47	455	421	438	433	vOC(11)+ $\beta$ CO(27)+ $\beta$ CCC(23)
48	-	-	399	400	$\beta$ OC(39)+ $\beta$ OCO(15)
49	-	-	378	368	$\tau$ HOCC(95)
50	-	325	313	313	$\beta$ OCO(14)+ $\beta$ CCC(41)
51	-	-	291	287	$\tau$ CCCC(11)+ $\gamma$ CCCC(47)
52	-	256	257	256	$\tau$ CCCC(42)+ $\tau$ COCC(26)+ $\gamma$ OCOC(11)
53	-	224	233	233	$\beta$ CCC(33)+ $\beta$ OCC(26)
54	-	-	204	206	$\tau$ HCCC(26)+ $\tau$ CCCC(32)
55	-	-	170	168	$\tau$ HCCC(26)+ $\tau$ CCCC(32)+ $\gamma$ CCCC(10)
56	-	-	105	103	$\tau$ CCCC(18)+ $\tau$ COCC(22)+ $\gamma$ CCCC(32)+ $\gamma$ OCOC(13)
57	-	82	93	91	$\tau$ CCCC(46)+ $\tau$ COCC(30)

v- stretching;  $\beta$ : in-plane-bending;  $\gamma$ : out-of-plane bending;  $\tau$ - torsion

## RESULTS AND DISCUSSION

### Molecular structure

The optimized molecular structure of 4MUB is shown in Fig.1. The optimization geometrical parameters of 4MUB obtained by the DFT/B3LYP/6-31G (2d,3p) and 6-311++G (2d,3p) as basis

sets are shown in Table 1. The structural data provided in Table 1 indicate that various bond lengths are found to be almost same at B3LYP/6-31G (2d,3p) and B3LYP/6-311++G(2d,3p) levels. However, the B3LYP/6-31G (2d,3p) level of theory, in general slightly over estimates bond lengths but it yields bond angles in excellent agreement with the B3LYP/6-311++G(2d,3p) method.

## Vibrational analysis

The molecule 4MUB under consideration belongs to C<sub>1</sub> point group symmetry and has 57 normal modes of fundamental vibrations. The FTIR and FT-Raman spectra of 4MUB are shown in Fig.2 and 3. The observed and calculated frequencies using B3LYP/6-31G (2d,3p) and 6-311++G (2d,3p) basis sets along with their probable assignments and potential energy distribution(PED) of the compound are summarized in Table 2. Comparison of the wavenumbers calculated by the DFT method using 6-31G (2d,3p) basis set with experimental values shown a very good agreement.

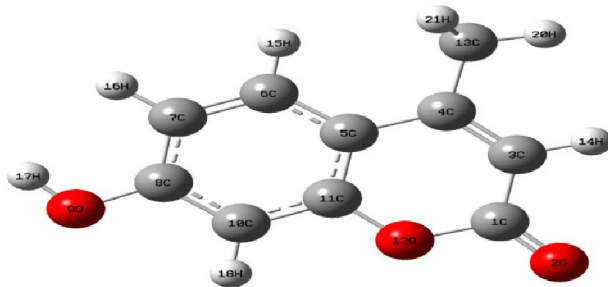


Fig.1. Optimized structure of 4MUB

### C–C vibrations

The bands between 1400 and 1650 cm<sup>-1</sup> in the aromatic and hetero aromatic compounds are assigned to carbon vibrations (Ilango, 2008). The actual positions are determined not by the nature of the substituents but rather by the form of the substitution around the aromatic ring. Moreover when C–N or more double modes are in conjugation the delocalization of  $\pi$ -electrons result in a transfer of some bond order to intervening single bonds and hence, there is full in the carbon–carbon stretching frequency. In this study the FTIR bands observed at 1694, 1610 and 1384 cm<sup>-1</sup> and Raman bands observed at 1691, 1614 and 1367 cm<sup>-1</sup> have been assigned to carbon–carbon stretching vibration. In the calculated values the stretching vibrations are observed at 1659 cm<sup>-1</sup> in 6-31G(2d,3p) and 1655 cm<sup>-1</sup> in 6-311++G(2d,3p) basis sets.

### C–H vibration

The substituted benzene like molecule gives rise to C–H stretching, C–H in-plane and C–H out-of-plane bending vibration. Aromatic compounds commonly exhibit multiple weak bands in the region 3200–3000 cm<sup>-1</sup> due to aromatic C–H stretching vibrations. The bands due to C–H in-plane bending vibrations interact somewhat with C–C stretching vibrations are observed as a number of bands in the region 1300–1000 cm<sup>-1</sup> (Gnanasambandan, 2013 and Rastogi, 2002). In this region the bands are not affected appreciable by the nature of the substituents. In the present investigations, the calculated bands identified at 3215, 3214, 3203 cm<sup>-1</sup> are assigned to C–H stretching vibrations. The IR and Raman bands observed at 1312, 1248, 1162 and 1313, 1161 cm<sup>-1</sup> were assigned to C–H in-plane bending vibrations.

### Methyl group vibrations

The compound under consideration 4MUB possess a CH<sub>3</sub> group in the side substitution chain. There are nine

fundamentals one can expect to a CH<sub>3</sub> group, namely the symmetrical stretching in CH<sub>3</sub> (CH<sub>3</sub> sym. stretch) and asymmetrical stretching (in plane hydrogen stretching mode); the symmetrical (CH<sub>3</sub> sym. deform) and asymmetrical (CH<sub>3</sub> asym. deform) deformation modes; in-plane rocking, out-of-plane rocking, twisting and bending modes (Gunasekaran, 2008). Each methyl group has three stretching vibrations, one being symmetric and other two asymmetric. The frequencies of asymmetric vibrations are higher than the symmetric one (Sharma, 1992). The theoretically computed values 2935 for CH<sub>3</sub> symmetric stretching and 3086 and 3128 cm<sup>-1</sup> for CH<sub>3</sub> asymmetric stretching shows an excellent agreement with the range allotted by Williams and Fleming (Dudley, 1988). The torsion vibrations are not observed in the FTIR and FT Raman spectrum because these appear at very low frequency. The observations in 4MUB are in agreement with theoretical results of similar compounds (Yadav, 2007).

### Carboxylic and carbonyl vibrations

The carbonyl stretching frequency has been most extensively studied by infrared spectroscopy (Socrates, 2001). This multiply bonded group is highly polar and therefore gives rise to an intense infrared absorption band. The carbon–oxygen double bond is formed by  $\pi$ – $\pi$  bonding between carbon and oxygen. Because of the different electro negativities of carbon and oxygen atoms, the bonding electrons are not equally distributed between the two atoms. The lone pair of electrons on oxygen also determines the nature of the carbonyl group. The carbonyl stretching vibrations are found in the region 1880–1700 cm<sup>-1</sup> (Gunasekaran, 2008). In 4MUB, the band appeared at 1825 cm<sup>-1</sup> (FT-IR) is belongs to C=O group. The corresponding calculated wavenumber is at 1830 cm<sup>-1</sup> using B3LYP/ 6-31G(2d,3p) basis set. The bands related to C=O bending mode are weak and complicated (Xiaopeng Xuan, 2011). Since it is a highly mixed mode as it is evident from Table 2. However, the band observed at 619 cm<sup>-1</sup> in both the FTIR and FT-Raman spectra is assigned to C=O in-plane bending modes. The frequencies calculated at 719 and 718 cm<sup>-1</sup> in B3LYP are assigned to C=O out-of-plane bending vibrations which are not observed in either of the spectra.

### O–H Vibrations

The carboxylic acid O–H stretching bands are weak in the Raman spectrum, so IR data are generally used. The O–H stretching is characterized by a very broad band appearing near about 3400 cm<sup>-1</sup> (Lin-vein, 1991 and Silverstein, 1981). On the other hand, the hydrogen bonding in the condensed phase with the other molecules makes vibrational spectra more complicated. Therefore, we could not observe the strong and sharp bands of the O–H vibration in the IR and Raman spectra. However, this band is calculated at 3639 cm<sup>-1</sup> in 6-31G(2d,3p) and at 3637 cm<sup>-1</sup> in 6-311++G(2d,3p) basis sets respectively. In the present work, the band at 3649 cm<sup>-1</sup> in IR is assigned as O–H stretching mode. In 4MUB, the O–H in-plane bending vibrations are assigned to 1261, 1209 cm<sup>-1</sup> in IR and 1269, 1212 cm<sup>-1</sup> in Raman spectra. The theoretically computed values at 1252, 1254 cm<sup>-1</sup> and 1198, 1196 cm<sup>-1</sup> in 6-31G (2d,3p) and 6-311++G(2d,3p) using B3LYP are in very good agreement with experimental values. As in Table 2, the in-

plane bending vibrations are combined with other vibrations. Donor–acceptor interactions: perturbation theory energy analysis NBO analysis provides the most accurate possible ‘natural Lewis structure’ picture of  $\phi$ , because all orbital details are mathematically chosen to include the highest possible percentage of the electron density. An useful aspect of the NBO method is that it gives information about interactions in both filled and virtual orbital spaces that could enhance the analysis of intra- and intermolecular interactions. The second order Fock matrix was carried out to evaluate the donor–acceptor interactions in the NBO analysis (Szafran *et al.*, 2007). The interactions result is a loss of occupancy from the localized NBO of the idealized Lewis structure into an empty non-Lewis orbital. For each donor (*i*) and acceptor (*j*), the stabilization energy  $E(2)$  associated with the delocalization  $i \rightarrow j$  is estimated as

$$E^{(2)} = \Delta E_{ij} = q_i \frac{F(i,j)^2}{\varepsilon_j - \varepsilon_i}$$

where  $q_i$  is the donor orbital occupancy,  $\varepsilon_i$  and  $\varepsilon_j$  are the diagonal elements and  $F(i, j)$  is the off diagonal NBO Fock matrix element.

Natural Bond Orbital analysis provides an efficient method for studying intra- and intermolecular bonding and interaction among bonds, and also provides a convenient basis for investigating charge transfer or conjugative interaction in molecular systems. Some electron donor orbital, acceptor orbital and the interacting stabilization energy resulted from the second-order micro-disturbance theory are reported (James, 2006 and Jun-na, 2005). The larger the  $E(2)$  value, the more intensive is the interaction between electron donors and electron acceptors, i.e. the more donating tendency from electron donors to electron acceptors and the greater the extent of conjugation of the whole system. Delocalization of electron density between occupied Lewis-type (bond or lone pair) NBO orbitals and formally unoccupied (antibond or Rydberg) non-Lewis NBO orbitals correspond to a stabilizing donor–acceptor interaction. NBO analysis has been performed on the molecule at the DFT/B3LYP/6-31G (2d,3p) level in order to elucidate the intramolecular, rehybridization and delocalization of electron density within the molecule are given in Table 3.

**Table 3. Second order perturbation theory analysis of Fock matrix in NBO analysis**

Donor( <i>i</i> )	Acceptor( <i>j</i> )	$E(2)^a$ (kJ/mol)	$E(j)-E(i)^b$ (a.u.)	$F(i, j)^c$ (a.u.)
$\pi(C3-C4)$	$\pi^*(C1-O2)$	22.44	0.29	0.078
$\pi(C5-C11)$	$\pi^*(C6-C7)$	23.35	0.28	0.074
$\pi(C6-C7)$	$\pi^*(C8-C10)$	22.33	0.29	0.074
$\pi(C8-C10)$	$\pi^*(C5-C11)$	25.84	0.28	0.078
LP(2) O2	$\sigma^*(C1-O12)$	40.46	0.56	0.136
LP(2) O9	$\pi^*(C8-C10)$	30.09	0.35	0.097
LP(2) O12	$\pi^*(C1-O2)$	36.00	0.35	0.100
LP(2) O12	$\pi^*(C5-C11)$	31.99	0.34	0.098
$\pi^*(C1-O2)$	$\pi^*(C3-C4)$	98.87	0.02	0.077
$\pi^*(C5-C11)$	$\pi^*(C3-C4)$	99.36	0.02	0.073

<sup>a</sup>  $E(2)$  means energy of hyper conjugative interaction (stabilization energy).

<sup>b</sup> Energy difference between donor and acceptor *i* and *j* NBO orbitals.

<sup>c</sup>  $F(i,j)$  is the fock matrix element between *i* and *j* NBO orbitals.

The intramolecular interaction is formed by the orbital overlap between bonding C–C, C–O, C–H, C–N and N–O antibond

orbital which results intramolecular charge transfer (ICT) causing stabilization of the system. These interactions are observed as increase in electron density (ED) in C–C, C–O, C–H, C–N and N–O antibonding orbital that weakens the respective bonds. The importance of hyper conjugation and electron density transfer from lone electron pairs of the Y atom to the X–H antibonding orbital in the X–H· · · Y system has been reported (Michalska, 1996). The intermolecular O–H· · · O hydrogen bonding is formed by the orbital overlap between the n(O) and  $\sigma^*(N-O)$  which results intramolecular charge transfer (ICT) causing stabilization of the H-bonded systems. Hence hydrogen bonding interaction leads to an increase in electron density (ED) of N–O antibonding orbital. The increase of the population of C–O antibonding orbital weakens the C–O bond. Thus the nature and strength of the intermolecular hydrogen bonding can be explored by studying the changes in electron density in vicinity of N· · · O hydrogen bonds. The NBO analysis of 4MUB clearly explains the evidence of the formation of strong H-bonded interaction between the LP(O) and  $\pi^*(C-C)$  antibonding orbitals. The stabilization energy  $E(2)$  associated with hyperconjugative interaction  $\pi^*(C5-C11) \rightarrow \pi^*(C3-C4)$ ,  $\pi^*(C1-O2) \rightarrow \pi^*(C3-C4)$ , LP2(O2)  $\rightarrow \sigma^*(C1-O12)$  and LP2(O12)  $\rightarrow \pi^*(C1-O2)$  are obtained as 99.36, 98.87, 40.46 and 36.00 kJ mol<sup>-1</sup> respectively are also listed in Table 3 which quantify the extend of intermolecular hydrogen bonding. The differences in  $E(2)$  energies are reasonably due to fact that the accrual of electron density in the C–O bond is not only drawn from the LP(O) of carbon-acceptor but also from the whole molecule.

### Non-linear optical (NLO) properties

NLO techniques are considered as one among the most structure-sensitive methods to study molecular structures and assemblies. Since the potential of organic materials for NLO devices have been proven, NLO properties of many of these compounds have been investigated by both experimental and theoretical methods (Varsanyi *et al.*, 1969). The efforts on NLO have been largely devoted to prepare first-order NLO materials using theoretical methods and exploring the structure–property relationships. Quantum chemical calculations have been shown to be useful in the description of the relationship between the electronic structure of the systems and its NLO response. The computational approach allows the determination of molecular NLO properties as an inexpensive way to design molecules by analyzing their potential before synthesis and to determine the higher order hyperpolarizability tensors of molecules.

Using 6-31G (2d,3p) basis set the calculated first order hyperpolarizability of 4MUB is  $5.1073 \times 10^{-30}$  e.s.u, which is 13 times that of urea. The calculated first order hyperpolarizability ( $\beta$ ) values are collected in Table 4. The theoretical calculation seems to be more helpful in the determination of particular components of  $\beta$  tensor than in establishing the real values of  $\beta$ . Domination of particular components indicates on a substantial delocalization of charges in those directions. It is noticed that in  $\beta_{xzz}$  (which is the principal dipole moment axis and is parallel to the charge transfer axis) direction, the biggest values of hyperpolarizability are noticed and subsequently delocalization of electron cloud is more in that direction.

**Table 4. NLO properties of 4MUB**

Parameters	B3LYP		Parameters	B3LYP	
	6-31G(2d,3p)	6-311++G(2d,3p)		6-31G(2d,3p)	6-311++G(2d,3p)
$\mu_x$	-3.6527	-3.7566	$\beta_{xxx}$	554.9960	676.9560
$\mu_y$	5.1721	5.7592	$\beta_{xyy}$	272.8030	308.6660
$\mu_z$	0.2587	0.3390	$\beta_{yyz}$	-56.3108	-63.5647
$\mu_{tot}$	6.3371	6.8844	$\beta_{yyz}$	26.2195	5.0734
$\alpha_{xx}$	182.182	194.302	$\beta_{xxz}$	-0.0602	0.0010
$\alpha_{xy}$	-8.325	-9.941	$\beta_{xyz}$	-0.0349	-0.0028
$\alpha_{yy}$	129.876	141.623	$\beta_{yzz}$	-0.0133	0.0196
$\alpha_{xz}$	0.008	0.036	$\beta_{xzz}$	-7.5028	-21.3613
$\alpha_{yz}$	-0.051	-0.109	$\beta_{yzz}$	30.0068	60.6278
$\alpha_{zz}$	53.912	70.633	$\beta_{zzz}$	0.0547	0.0380
$\alpha_{tot}(\text{esu})$	$1.8078 \times 10^{-23}$	$2.0083 \times 10^{-23}$	$\beta_{tot}(\text{esu})$	$5.1073 \times 10^{-30}$	$6.0513 \times 10^{-30}$
$\Delta\alpha(\text{esu})$	$4.9608 \times 10^{-23}$	$5.2357 \times 10^{-23}$			

**Table 5. Mulliken atomic charges of 4MUB**

Atoms	B3LYP		Atoms	B3LYP	
	6-31G(2d,3p)	6-311++G(2d,3p)		6-31G(2d,3p)	6-311++G(2d,3p)
C1	0.432897	0.635766	O12	-0.368073	-0.579819
O2	-0.344980	-0.457052	C13	-0.210848	-0.165653
C3	-0.203075	-0.584365	H14	0.033137	0.027943
C4	0.204429	1.122893	H15	0.010521	0.007928
C5	0.111093	0.304396	H16	-0.005321	-0.011690
C6	-0.126164	0.131930	H17	0.176712	0.391919
C7	-0.089684	0.037475	H18	0.036971	0.039989
C8	0.408670	0.031351	H19	0.056805	0.048768
O9	-0.366668	-0.555275	H20	0.018303	0.058521
C10	-0.171387	-0.500338	H21	0.074979	0.060619
C11	0.321683	-0.045309			

**Table 6. UV-Vis excitation energy ( $\Delta E$ ) of 4MUB**

States	TD-B3LYP/6-31G(2d,3p)				Expt.	Major Contributions		
	Gas phase		Ethanol					
	$\lambda_{cal}$	E(eV)	$\lambda_{cal}$	E(eV)				
S1	318.9	4.3672	321.96	4.2321	325	H $\rightarrow$ L(62%), H-1 $\rightarrow$ L(15%)		
S2	262.4	4.4844	260.82	4.5612	265	H-1 $\rightarrow$ L(40%), H-2 $\rightarrow$ L(19%)		
S3	250.7	4.7197	248.85	4.7898	253	H+2 $\rightarrow$ L(23%), H $\rightarrow$ L+1(48%)		

**Table 7. Molecular properties of 4MUB**

Molecular properties	B3LYP		Molecular properties	B3LYP	
	6-31G(2d,3p)	6-311++G(2d,3p)		6-31G(2d,3p)	6-311++G(2d,3p)
$\epsilon_{HOMO}(\text{eV})$	-6.08533	-6.475816	Chemical hardness( $\eta$ )	2.267275	2.253392
$\epsilon_{LUMO}(\text{eV})$	-1.55078	-1.969031	Chemical potential( $\mu$ )	-3.818055	-4.222423
$\epsilon(H-L)$ (eV)	-4.53455	-4.506785	Electronegativity( $\chi$ )	3.818055	4.222423
Ionization potential(I)	6.08533	6.475816	Electrophilicity index( $\omega$ )	7.288771	8.914430
Electron affinity(A)	1.55078	1.969031	Softness(S)	0.441058	0.443775

**Table 8. Condensed Fukui functions and local softness of 4MUB**

Atoms	$f_k^-$	$f_k^+$	$f_k^0$	$S_k^- = Sf_k^-$	$S_k^+ = Sf_k^+$	$S_k^0 = Sf_k^0$
C1	0.06299	0.03015	0.04657	0.01389	0.00665	0.01027
O2	0.09531	0.09006	0.09268	0.02101	0.01986	0.02044
C3	0.06396	0.08069	0.07032	0.01410	0.01779	0.01550
C4	0.03742	0.00299	0.02021	0.00825	0.00066	0.00445
C5	0.00082	0.03784	0.01933	0.00018	0.00834	0.00426
C6	0.05316	0.02337	0.03826	0.01172	0.00515	0.00843
C7	0.00772	0.04799	0.02786	0.00170	0.01058	0.00614
C8	0.05207	0.03467	0.04337	0.01148	0.00764	0.00956
O9	0.04227	0.08917	0.06572	0.00932	0.01966	0.01449
C10	0.04035	0.03355	0.03695	0.00889	0.00756	0.00814
C11	0.01845	0.03745	0.02795	0.00406	0.00825	0.00616
O12	0.02821	0.03534	0.03175	0.00622	0.00779	0.00700
C13	-0.01675	-0.01512	-0.01593	-0.00369	-0.00333	-0.00351
H14	0.09608	0.08175	0.08892	0.02118	0.01803	0.01960
H15	0.07468	0.06763	0.07116	0.01647	0.01491	0.01569
H16	0.07972	0.08384	0.08178	0.01758	0.01848	0.01803
H17	0.03228	0.04004	0.03616	0.00711	0.00883	0.00797
H18	0.07764	0.07270	0.07517	0.01712	0.01603	0.01657
H19	0.05262	0.04038	0.04650	0.01160	0.00890	0.01025
H20	0.05247	0.04491	0.04869	0.01157	0.00990	0.01073
H21	0.04843	0.04052	0.04447	0.01068	0.00893	0.00980

The maximum  $\beta$  value may be due to  $\pi$ -electron cloud movement from donor to acceptor which makes the molecule highly polarized and the intramolecular charge transfer possible. The presence of intra-molecular charge transfer is confirmed with the vibrational spectral analysis.

### Molecular electrostatic potential

Molecular electrostatic potential and electrostatic potential are useful quantities to illustrate the charge distributions of molecules and used to visualize variably charged regions of a molecule. Therefore, the charge distributions can give information about how the molecules interact with another molecule. Molecular electrostatic potential is widely used as a reactivity map displaying most probable regions for the electrophilic attack of charged point-like reagents on organic molecules (Politzer, 1981).

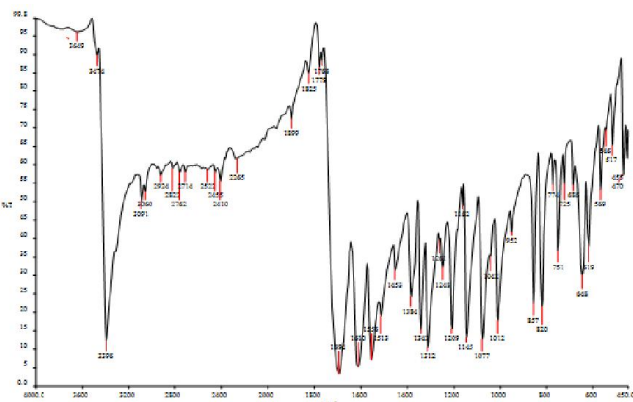


Fig.2. Experimental FT-IR spectrum of 4MUB

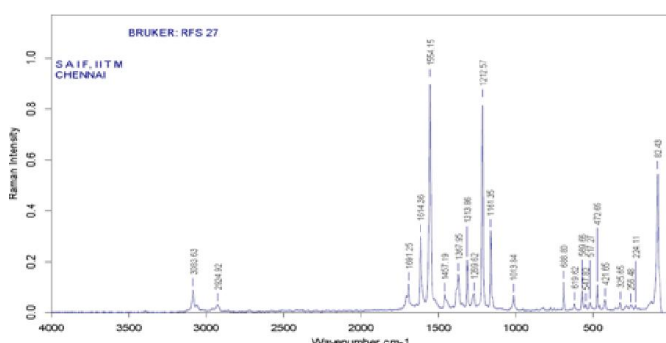


Fig.3. Experimental FT-Raman spectrum of 4MUB

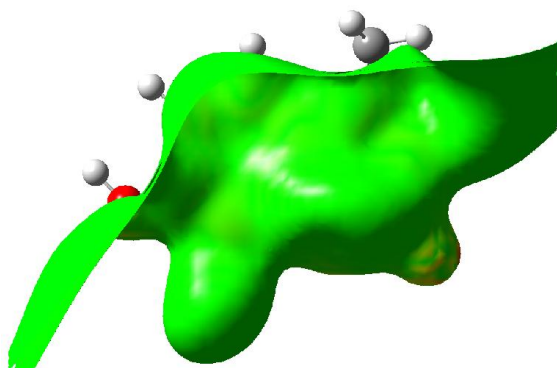


Fig.4. Molecular electrostatic potential of 4MUB

The molecular electrostatic potential  $V(r)$  that is created in the space around a molecule by its nuclei and electrons is well established as a guide to molecular reactive behaviour. It is defined by:

$$V(r) = \sum_A \frac{Z_A}{(R_A - r)} - \int \frac{\rho(r')}{(r' - r)} dr'$$

in which  $Z_A$  is the charge of nucleus A, located at  $R_A$ ,  $\rho(r')$  is the electronic density function for the molecule and  $r'$  is the dummy integration variable (Politzer, 1985). At any given point  $r(x, y, z)$  in the vicinity of a molecule, the molecular electrostatic potential (MEP),  $V(r)$  is defined in terms of the interaction energy between the electrical charge generated from the molecule electrons and nuclei and a positive test charge (a proton) located at  $r$  (Politzer, 2002).

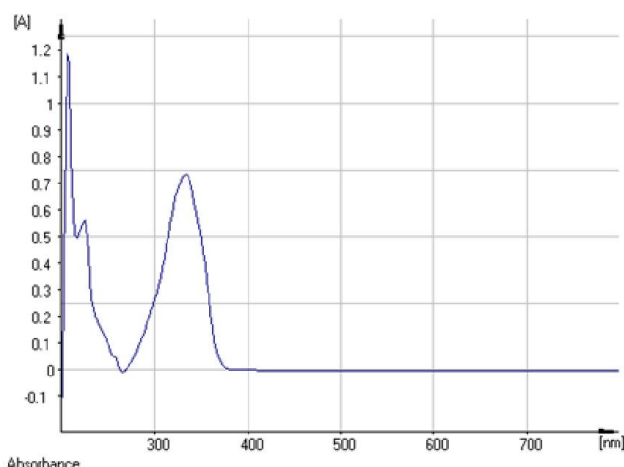


Fig. 5. UV-Visible spectra of 4MUB

In the graphic of total electron density surface mapped with the electrostatic potential, the sign of the electrostatic potential in a surface region is determined by the predominance of negative charges contribution or positive charges contribution. Accordingly, it is possible to identify regions more susceptible to approximation of electrophilic molecules or nucleophilic molecules, so the molecular electrostatic potential map is commonly used as reactivity map. The molecular electrostatic potential for 4MUB in 3D plot is illustrated in Fig. 4.

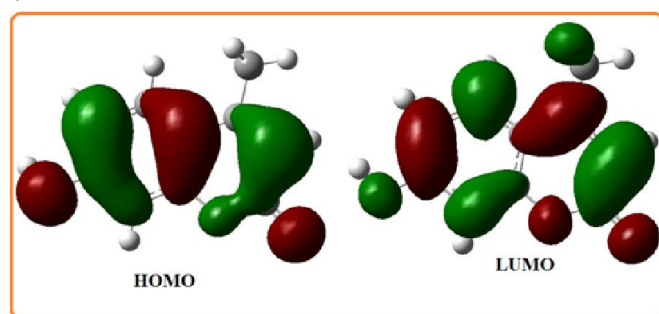


Fig.6. Frontier molecular orbitals of 4MUB

The importance of total electron density surface mapped with the electrostatic potential lies in the fact that it simultaneously displays molecular size, shape, as well as positive or negative electrostatic potential regions in terms of color grading and is

very useful in research of molecular structure with its physiochemical property relationship (Okulik, 2005). The different values of the electrostatic potential are represented by different colors. The range values for the color scale of the mapped MESP should be symmetrical to allow easily identification of negative (red) and the positive (blue) potential regions. The use of a symmetrical potential scale values eases the recognition of positive, zero or negative regions. In GaussView visualizing program (Frisch, 2000), the following spectral color scheme is used. So potential increases in the order: red < orange < yellow < green < blue. Therefore red indicates negative regions, blue indicates positive regions, while green appears over zero electrostatic potential regions. It is accepted that the negative (red) and the positive (blue) potential regions in the mapped MESP represent regions susceptible to approach electrophilic molecules or nucleophilic molecules, respectively. It can be seen that the most possible sites for electrophilic attack is C1. Negative regions in the studied molecule are found around the O12 atom indicating a possible site for nucleophilic attack. According to these calculated results, the MEP map shows that the negative potential sites are on electronegative atoms as well as the positive potential sites are around the hydrogen atoms.

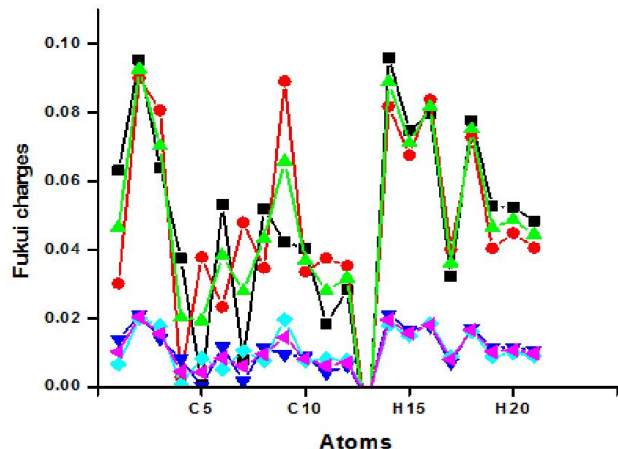


Fig. 7. Fukui function charges of 4MUB

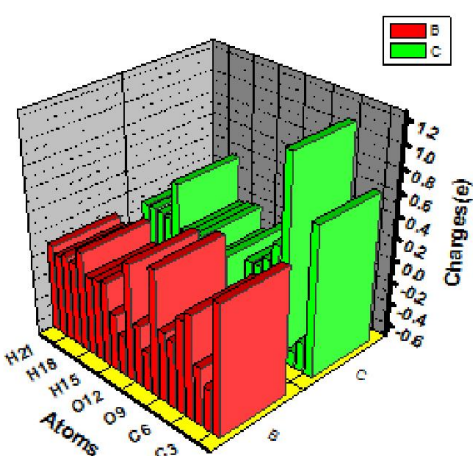


Fig. 8. Mulliken atomic charges of 4MUB

#### UV spectrum and Frontier molecular orbital analysis

Ultraviolet spectra analysis of 4MUB are researched by theoretical calculation and experiment. The electronic

absorption spectrum of the title molecule is measured in both gas phase and ethanol. The excitation energies, absorbance and major contributions for the title molecule at the optimized geometry are obtained in the framework of DFT calculations by using the B3LYP/6-31G (2d,3p) method. The UV spectra of 4MUB is shown in Fig. 5. The predicted UV spectra results are depicted in Table 6 such as absorption wavelengths ( $\lambda$ ), excitation energies ( $\Delta E$ ) and major contributions of the transitions and assignments of electronic transitions. From the experimental and theoretical UV spectra, the absorption bands are coincides at 321.96 and 262.48 nm for 4MUB. The HOMO and LUMO are named as frontier molecular orbitals (FMOs). The FMOs play an important role in the optical and electric properties, as well as in quantum chemistry and UV–Vis spectra (32). The HOMO represents the ability to donate an electron, LUMO as an electron acceptor represents the ability to obtain an electron. The energy gap between HOMO and LUMO determines the chemical potential, electronegativity, electrophilicity index and chemical hardness and softness of a molecule. The plots of MOs have been drawn and given in Fig. 6. As can be seen from Fig. 6, the energy gap between HOMO and LUMO is 4.5345eV for 4MUB molecule. From Table 6, the largest contribution to charge transition in 318.90nm (theoretical value) is from the HOMO to the LUMO with 62%. The largest contribution for 262.48 nm is belonged to transitions which  $H - 1 \rightarrow L$  with 40% and  $H-2 \rightarrow L$  with 19%. Also, in 250.70 nm,  $H \rightarrow L+1$  transition has the contribution with 48%.

#### Molecular Transport Properties

The other electronic properties as the chemical potential ( $\mu$ ), electronegativity ( $\chi$ ), electrophilicity index ( $\omega$ ) and chemical hardness ( $\eta$ ) have given in Table 7. The  $\eta$ ,  $\chi$  and  $\mu$  are important tools to study the order of stability of molecular systems. Using HOMO and LUMO energies, the  $\eta$  and  $\mu$  have been calculated. The chemical hardness and the chemical potential are given by the following expression,  $\eta = (I-A)/2$   $\mu = -(I+A)/2$ . The  $\omega^2$ , which measures the stabilization energy, has been given by the following expression, in terms of electronic chemical potential and the chemical hardness:  $\omega = \mu^2/2$  electronegativity ( $\chi$ ),  $\chi = (I+A)/2$  or  $\chi = -\mu$  where I and A are ionization potential and electron affinity of a molecular system.

#### Local reactivity descriptors

The most relevant local descriptor of reactivity is the Fukui function. Yang and Parr (Yang, 1985) proposed a finite difference to calculate Fukui function indices. In a molecular system,  $f_k^+$  measures the change in density when the molecule gains electrons and it corresponds to reactivity with respect to nucleophilic attack. Whereas,  $f_k^-$  corresponds to reactivity with respect to electrophilic attack when the molecule losses electrons. In addition to fukui function the localsoftness ( $S_k^+$ ,  $S_k^-$ ,  $S_k^0$ ) is also used to describe the reactivity of the molecular system. And the Softness(S) is found by the following expression  $S = \frac{1}{E_L - E_H}$  where  $E_L$  and  $E_H$  refers the energies of the LUMO and HOMO respectively. Fukui function and local softness for selected atomic sites in 4MUB have been listed in

the Table 8. From the values reported in the Table 8, the highest nucleophilic attack is on O<sub>2</sub>. The other nucleophilic attack order was found to be O<sub>9</sub> > H<sub>16</sub> > H<sub>14</sub> > C<sub>3</sub> > H<sub>18</sub>. The sites for electrophilic attack were H<sub>14</sub>, O<sub>2</sub>, and H<sub>16</sub>. The radial attack was on O<sub>2</sub>, H<sub>14</sub> and H<sub>16</sub>. S<sub>k</sub><sup>+</sup>, S<sub>k</sub><sup>-</sup> and S<sub>k</sub><sup>0</sup> predicts the most nucleophilic and electrophilic and radial attack in a molecule is the one which has the S<sub>k</sub><sup>+,0</sup> value, in turn is the softest region in a molecule. The plot of fukui function charges is shown in Fig.7.

### Mulliken atomic charges

The computation of the reactive atomic charges play an important role in the application of quantum mechanical calculations for the molecular system. Mulliken atomic charges are calculated by DFT/B3LYP method with 6-31G(2d,3p) and 6-311++G(2d,3p) basis sets. To make comparison, between the two basis sets, the Mulliken atomic charges of 4MUB are tabulated in Table 5. We have plotted the graph of these values as shown in Fig. 8. All hydrogen atoms have a net positive charge except H<sub>16</sub>. For 4MUB, the maximum negative charges belong to O<sub>12</sub> atom and the value is -0.3680. The maximum positive charge belonging to C<sub>1</sub> atom is 0.4328.

### Conclusion

This study demonstrates that scaled DFT (B3LYP) calculations are powerful approach for understanding the vibrational spectra of the title molecule. The FT-IR, FT-Raman along with UV-spectral studies of 4MUB were carried out for the first time. A Complete vibrational and molecular structure analysis have been performed based on the quantum mechanical approach. The difference between the observed and scaled wavenumber values of most of the fundamentals are very small. Therefore, the assignments made at DFT level of theory with only reasonable deviations from the experimental values seem to be correct. NBO analysis indicating the strong intramolecular hyperconjugative interaction within the molecule and stability of the molecule. The calculated first order hyperpolarizability of 4MUB is much greater than that of urea. This indicates that the title compound is best material for NLO applications. The Mulliken charges and natural atomic charges of the title molecule have been studied by DFT methods. The calculated HOMO and LUMO energies can be used to estimate the ionization potential, electron affinity, electronegativity, electrophilicity index, hardness, softness and chemical potential. The predicted MEP shows the negative electrophilic potential regions are mainly localized over the oxygen atoms. Fukui function, local softness and electrophilicity indices for selected atomic sites in 4MUB have also been calculated.

### REFERENCES

- Arjunan, V. Sakiladevi, S. Marchewka, M.K. Mohan, S. Spectrochim. 2013. *Acta*, 109 79-89
- Dudley, N.B. Williams, H. and Ian Fleming, 1988. Spectroscopic Methods in Organic Chemistry, Tata McGraw-Hill, UK.
- Fleming, I. 1976. Frontier Orbitals and Organic Chemical Reactions, Wiley, London.
- Frisch, A. Nielson, A.B. Holder, A.J. GAUSSVIEW User Manual, Gaussian Inc., Pittsburgh, PA, 2000.
- Gaussian 03 program, Gaussian Inc., Wallingford CT, 2004.
- Gnanasambandan, T. Gunasekaran, S. Seshadri, S. 2013. Spectrochim. Acta A 112 52-61.
- Gunasekaran, S. Kumaresan, S. Arunbalaji R. and S.Srinivasan, 2008. *J.Chem. Sci.*, Volume 120, Issue 3 315-324.
- Ilango, G. Arivazhagan, M. Joseph Prince, J. Balechandran, V. 2008. *Ind. J. Pure Appl. Phys.*, 46 698.
- James, C. Raj, A.A. Reghunathan, R. Joe, I.H. Jayakumar, V.S. 2006. *J. Raman Spectrosc.*, 37,2 1381-1392.
- Jamroz, M.H. Vibrational Energy Distribution Analysis, VEDA 4 Computer Program, Poland, 2004.
- Jun-na, LIU Zhi-rang, CHEN Shen-fang, YUAN Zhejiang 2005. *J. Univ. Sci.* 6B 584-589.
- Krishnakumar, V. Mathammal, R. Muthunatesan, S. 2008. Spectrochim. Acta, 70A 210–216.
- Lin-vein, D. Colthup, N.B. Fateley, W.G. Grasselli, J.G. 1991. The Handbook of Infrared and Raman characteristic frequencies of organic molecules, Academic Press, SanDiego.
- Michalska, D. Bienko, D.C. Bienko, A.J.A. Latajka, Z. *J. Phys. Chem.*, 100, 45 (1996) 17789-17790.
- National Institute of Standards and Technology. Vibrational Frequency Scaling Factors on the Web. <<http://srdata.nist.gov/cccdb/vsf.asp>> (accessed 24.09.07)
- Okulik, N. Jubert, A.H. 2005. *Internet Electron. J. Mol. Des.*, 4 17–30.
- Politzer, P. Laurence, P.R and Jayasuriya, K. 1985. Molecular electrostatic potentials: an effective tool for the elucidation of biochemical phenomena, in: J. McKinney (Ed.), Structure Activity Correlation in Mechanism Studies and Predictive Toxicology, Environ. Health Perspect, vol. 61, pp. 191–202.
- Politzer, P. Murray, J.S. 2002. *Theor. Chem. Acc.* 108 134–142.
- Politzer, P. Truhlar, D.G. (Eds.), Chemical Application of Atomic and Molecular Electrostatic Potentials, Plenum, New York, 1981.
- Prabavathi, N. Senthil Nayaki, N. *Environ. J. Nanotechnol.*, Volume 3, No.2 pp. 108-121.
- Rastogi, K. Palafox, M.A. Tanwar, R.P Mittal, L. 2002. Spectrochim. Acta, A 58, 9 1987-2004.
- Schlegel, H.B. *J. Comput. Chem.* 3 (1982) 214–218.
- Sharma, M.K. Medhi, K.C. 1992. *Indian J Phys.*, 66B,1 59–64.
- Silverstein, M. Clayton Basseler, G. Morill, C. 1981. Spectrometric Identification of organic compounds, Wiley, Newyork.
- Sivasubramanian, M. 2012. *Int. J Engg. Research & Technology*, 1(7), 278-288
- Socrates, G. 2001. Infrared and Raman Characteristic Group Frequencies, third ed., Wiley, New York.
- Subramanian, M.K., Anbarasan, P.M., Manimegalai, S. 2010. *Pramana-Journal of Physics*, 74, 845-860
- Szafran, M. Komasa, A. Adamska, E.B. 2007. *J. Mol. Struct. (THEOCHEM)* 827 101-107.
- Udaya Sri, N. Chaitanya, K. Prasad, M.V.S. Veeraiah, V. 2012. Veeraiah, A. Spectrochim. Acta, 97728-736

- 
- Varsanyi, G. *Vibrational Spectra of Benzene Derivatives*, Academic Press, New York, 1969.
- Xiaopeng Xuan, Xinsheng wang, 2011. Na wang, *Spectrochim. Acta* 79A 1091-1110.
- Yadav, B S Israt Ali, Pradeep kumar and Prrti Yadav, 2007  
*Indian J Pure & Appl. Phys.*, Vol. 45 979-983.
- Yang, W. Parr, R. 1985. *Proc. Natl. Acad. Sci (Chem.)* 82 6723-6726.

\*\*\*\*\*